General Disclaimer

One or more of the Following Statements may affect this Document

- This document has been reproduced from the best copy furnished by the organizational source. It is being released in the interest of making available as much information as possible.

- This document may contain data, which exceeds the sheet parameters. It was furnished in this condition by the organizational source and is the best copy available.

- This document may contain tone-on-tone or color graphs, charts and/or pictures, which have been reproduced in black and white.

- This document is paginated as submitted by the original source.

- Portions of this document are not fully legible due to the historical nature of some of the material. However, it is the best reproduction available from the original submission.

Produced by the NASA Center for Aerospace Information (CASI)

NASA Technical Memorandum 73959

A RING-SOURCE MODEL FOR JET NOISE

Lucio Maestrello

APRIL 1978

NASA

National Aeronautics and
Space Administration

Langley Research Center
Hampton, Virginia 23665

SUMMARY

An analytical model consisting of two ring sources is developed to
study the direct radiation of jet noise in terms of correlation, coherence,
and phase and also to aid in solving the inverse radiation problem of
determining the noise source in terms of far-field measurements. The rings
consist of discrete sources which are either monopoles or quadrupoles with
Gaussian profiles. Only adjacent sources, both within the rings and between
rings, are correlated. Results show that from the far-field information one
can determine when the sources are compact or noncompact with respect to
the acoustic wavelength and distinguish between the types of sources. In
addition, from the inverse radiation approach one can recover the center of
mass, the location and separation distance of the ring and the diameters.

INTRODUCTION

This paper addresses a solution of the direct and inverse problems in
the radiation of sound from randomly fluctuating sources on two rings. This
effort resulted from the fact that even a well designed experiment cannot
be free of ambiguity and as such it is shown that a parallel study using a
model is essential in minimizing the experimental uncertainties. In addition,
the recovery of the unknown source distribution on a jet is more easily
obtainable from an analytical model, which is by far a superior tool than
from the measurements.

The approach utilizes space-time correlation of the far-field sound which
clearly provides more information of physical importance than a single point
data. The first theory and experimental work on two point correlation from a
jet were reported in references 1 to 3, and for the inverse approach in
references 4 and 5. Several other papers have been written discussing the

recovery of the unknown source field in an application to the jet noise problem. The most recent ones are given in references 6 to 10.

Conceivably, there are many possible ways to utilize the radiation data to yield some information about the source field. In general, however, the common difficulty in dealing with inverse problems in physical sciences lies in the fact that they are ill-posed in Hadamark sense (ref. 11). The present approach was designed to fit the physical problem under consideration; that is, treating the direct and inverse stochastic problem in a uniform media for jet application.

The first part of the analysis contains the direct approach and numerical results on two ring sources. The sources in the rings are random and coupled with Gaussian profiles. To better distinguish the type of singularities, two types were used: (a) random monopole and (b) random quadrupole. The second part of the paper contains the inverse approach accompanied by the numerical results and the description of the method to determine the basic geometry with compactness and identification.

ANALYSIS

The source model consists of two rings, centered on and, perpendicular to the jet axis. Each ring is made up of a finite number of discrete sources which may be either monopoles or quadrupoles. The rings have different radii, simulating the spreading of the jet. The sources in the rings are random in time with Gaussian profile. Only adjacent sources, both within the rings as well as between rings, are correlated.

In order to investigate the phase effects arising from different types of sources, two types of sources are used: (a) random monopoles and (b) random quadrupoles.

The variables in the model are the number of sources in the rings, distance between rings, and ring radius. The sources can either be real or complex. A simple interpretation for complex sources in the direction of the jet can be given in terms of convection effects. The sources, however, can also be interpreted as the Lighthill sources, that is, the sources of an equivalent medium at rest.

A. Direct Radiation

The geometry of the model is given in figure 1. The symbol $q_{i,j}(t)$ denotes the source placed at an angle ϕ_j in the i-th ring with $\phi_j = (j - 1)\Delta$, $j = 1 \ldots N$ and $\Delta = 2\pi/N$. N is the number of sources which are equally spaced over the rings of radii a_i for $i = 1, 2$. The ring with radius a_2 is larger than the ring with radius a_1. The two rings are placed at distance ℓ_1 and ℓ_2, respectively from the exit of an ideal jet.

	Position			Strength
	x	y	z	
1st Ring	$S_{1,j}(\ell_1,$	$a_1 \cos \phi_j,$	$a_1 \sin \phi_j)$	$q_{1,j}(t)$
2nd Ring	$S_{2,j}(\ell_2,$	$a_2 \cos \phi_j,$	$a_2 \sin \phi_j)$	$q_{2,j}(t)$

$$(1)$$

$\vec{L}_k$ denotes the far-field position vector of the field points with $k = 1, 2$. In spherical coordinates, $\vec{L}_1(r_1, \theta_1, \phi_1)$ and $\vec{L}_2(r_2, \theta_2, \phi_2)$. We set $r_1 = r_2 = r$, in which case the distance between a point on the ring and a point in the far-field is given by

$$|l_k - S_{ij}| = \sqrt{r^2 + \ell_i^2 + a_i^2 - 2r\ell_i \cos \theta_k - 2ra_i \sin \theta_k \cos(\phi_j - \phi_k)}$$

$$\sim r - \ell_i \cos \theta_k - a_i \sin \theta_k \cos(\phi_j - \phi_k) \tag{2}$$

We denote the self correlation of the random source by $Q_1(\tau)$ and $Q_2(\tau)$. Therefore,

$$\rho^2 < q_{1,j}(t)q_{1,j}(t + \tau) > = Q_1(\tau)$$

$$\rho^2 < q_{2,j}(t)q_{2,j}(t + \tau) = Q_2(\tau)$$

We assume that only the adjacent sources are correlated:

$$\rho^2 < q_{1,j}(t)q_{1,k}(t + \tau) > = Q_{1,1}(\tau)\left[\delta_{1,|j-k|}\right]$$

$$\rho^2 < q_{2,j}(t)q_{2,k}(t + \tau) > = Q_{2,2}(\tau)\left[\delta_{1,|j-k|}\right]$$

$$\rho^2 < q_{1,j}(t)q_{2,j}(t + \tau) > = Q_{1,2}(\tau)$$

$$\rho^2 < q_{1,j}(t + \tau)q_{2,j}(t) > = Q_{1,2}(-\tau)$$

$$\rho^2 < q_{1,j}(t)q_{2,k}(t + \tau) > = Q_{1,2}^*(\tau)\left[\delta_{1,|j-k|}\right]$$

$$\rho^2 < q_{2,k}(t)q_{1,j}(t + \tau) > = Q_{1,2}^*(-\tau)\left[\delta_{1,|j-k|}\right]$$

We implied that $q_{i,0} = q_{i,N}$ and $q_{i,N+1} = q_{i,1}$. Note that Q_1, Q_2, $Q_{1,1}$ and $Q_{2,2}$ are even functions of τ.

The pressure P_k due to source $S_{i,j}$ is

$$P_k = \rho \dot{q}_{i,j}\left(t - \frac{|L_k - S_{i,j}|}{c_o}\right)\bigg/ |L_k - S_{i,j}|$$

where $\dot{q}_{i,j}(t) = \frac{d}{dt} q_{i,j}$. The time derivative is used to convert into
unit of pressure. The far-field cross correlation function is:

$$<P_1(t)P_2(t + \tau)> = \rho^2 <\left\{\sum_{i=1}^{2}\sum_{j=1}^{N} \dot{q}_{i,j}\left(t - \frac{|L_1 - S_{i,j}|}{c_o}\right)\bigg/|L_1 - S_{i,j}|\right\}$$

$$\left\{\sum_{k=1}^{2}\sum_{m=1}^{N} \dot{q}_{k,m}\left(t + \tau - \frac{|L_2 - S_{k,m}|}{c_o}\right)\bigg/|L_2 - S_{k,m}|\right\}>$$

$$\sim \frac{\rho^2}{r^2} <\left\{\sum_{i=1}^{2}\sum_{j=1}^{N} \dot{q}_{i,j}(t)\sum_{k=1}^{2}\sum_{m=1}^{N} \dot{q}_{k,m}\left(t + \tau - \mu_{i,j,k,m}\right)\right\}> \quad (3)$$

where $\mu_{i,j,k,m} = \left\{-|L_1 - S_{i,j}| + |L_2 - S_{k,m}|\right\}\bigg/c_o$

$$= \left\{\left[\ell_i \cos\theta_1 + a_i \sin\theta_1 \cos(\phi_j - \phi_1)\right]\right\}\bigg/c_o$$

$$- \left\{\left[\ell_k \cos\theta_2 + a_k \sin\theta_2 \cos(\phi_m - \phi_2)\right]\right\}\bigg/c_o \quad (4)$$

1. <u>Rings with monopoles</u>.- The far-field cross correlation for monopole
sources can be written as follows

$$\frac{r^2}{\rho^2} < P_1(t)P_2(t + \tau) > = - \frac{r^2}{\rho^2}\frac{d^2}{d\tau^2} R_{1,2}(\tau) \quad (5)$$

where

$$R_{1,2}(\tau) = \sum_{j=1}^{N} Q_1\left(\tau - \mu_{1j,1j}\right) + \sum_{j=1}^{N}\left[Q_{1,1}\left(\tau - \mu_{1j,1,j+1}\right) + Q_{1,1}\left(\tau - \mu_{1j,1,j-1}\right)\right]$$

$$+ \sum_{j=1}^{N} Q_{1,2}\left(\tau - \mu_{1j,2j}\right) + \sum_{j=1}^{N}\left[Q_{1,2}^{\star}\left(\tau - \mu_{1j,2,j+1}\right) + Q_{1,2}^{\star}\left(\tau - \mu_{1j,2,j-1}\right)\right]$$

$$+ \sum_{j=1}^{N} Q_{1,2}\left(-\tau + \mu_{2j,1j}\right) + \sum_{j=1}^{N}\left[Q_{1,2}^{\star}\left(-\tau - \mu_{2j,1,j+1}\right) + Q_{1,2}^{\star}\left(-\tau + \mu_{2j,1,j-1}\right)\right]$$

$$+ \sum_{j=1}^{N} Q_2\left(\tau - \mu_{2j,2j}\right) + \sum_{j=1}^{N}\left[Q_{2,2}\left(\tau - \mu_{2j,2,j+1}\right) + Q_{2,2}\left(\tau - \mu_{2j,2,j-1}\right)\right]$$

We make use of the relationship

$$< \dot{q}(t)\dot{q}(t + \tau) > = \frac{d}{d\tau} < \dot{q}(t)q(t + \tau) > = -\frac{d}{d\tau} < q(t)\dot{q}(t + \tau) >$$

$$= \frac{d^2}{d\tau^2} < q(t)q(t + \tau) > = -\frac{d^2}{d\tau^2} Q(\tau) \tag{6}$$

The Fourier transform of $R_{1,2}(\tau)$ is

$$\hat{R}_{1,2}(\omega) = \hat{Q}_1(\omega)\sum_{1}^{N} e^{i\omega\mu_{1,j,1,j}}$$ Uncorrelated sources on the first ring

$$+ \hat{Q}_2(\omega)\sum_{1}^{N} e^{i\omega\mu_{2,j,2,j}}$$ Uncorrelated sources on the second ring

$$+ \hat{Q}_{1,1}(\omega)\sum_{1}^{N}\left[e^{i\omega\mu_{1,j,1,j+1}} + e^{i\omega\mu_{1,j+1,1,j}}\right]$$ Correlation between $S_{1,j}$; $S_{1,j+1}$

$$+ \hat{Q}_{2,2}(\omega)\sum_1^N \left[e^{i\omega\mu_{2,j,2,j+1}} + e^{i\omega\mu_{2,j+1,2,j}} \right] \qquad \text{Correlation between } S_{2,j}; S_{2,j+1}$$

$$+ \hat{Q}_{1,2}(\omega)\sum_1^N e^{i\omega\mu_{1,j,2,j}} + \hat{Q}_{1,2}(-\omega)\sum_1^N e^{i\omega\mu_{2,j,1,j}} \qquad \text{Correlation between } S_{1,j}; S_{2,j}$$

$$+ \hat{Q}^*_{1,2}(\omega)\sum_1^N e^{i\omega\mu_{1,j,2,j+1}} + \hat{Q}^*_{1,2}(-\omega)\sum_1^N e^{i\omega\mu_{2,j+1,1,j}} \qquad \text{Correlation between } S_{1,j}; S_{2,j+1}$$

$$+ \hat{Q}^*_{1,2}(\omega)\sum_1^N e^{i\omega\mu_{1,j,2,j-1}} + \hat{Q}^*_{1,2}(-\omega)\sum_1^N e^{i\omega\mu_{2,j-1,1,j}} \qquad \text{Correlation between } S_{1,j}; S_{2,j-1} \qquad (7)$$

For the computation of the cross spectral density, $-(r^2/\rho^2\omega^2)\hat{R}_{1,2}(\omega)$, one needs the six correlation functions of the sources; i.e., Q_1, Q_2, $Q_{1,1}$, $Q_{2,2}$, $Q_{1,2}$, and $Q^*_{1,2}$ or their Fourier transforms.

For the purpose of computing the cross correlation $R_{1,2}(\tau)$ let us assume that $Q_1(\tau)$, $Q_2(\tau)$, $Q_{1,1}(\tau)$, $Q_{2,2}(\tau)$, $Q_{1,2}(\tau)$, and $Q^*_{1,2}(\tau)$ have Gaussian form which has frequently been used in the past (refs. 12 and 13).

$$Q_1(\tau) = e^{-(\gamma_1\tau)^2}$$

$$Q_2(\tau) = e^{-(\gamma_2\tau)^2}$$

$$Q_{1,1}(\tau) = \frac{1}{2}\left[e^{-\gamma_1^2\left(\tau - \frac{\pi}{N}\psi_1\right)^2} + e^{-\gamma_1^2\left(\tau + \frac{\pi}{N}\psi_1\right)^2} \right]$$

8

$$Q_{2,2}(\tau) = \frac{1}{2}\left[e^{-\gamma_2^2\left(\tau - \frac{\pi}{N}\psi_2\right)^2} + e^{-\gamma_2^2\left(\tau + \frac{\pi}{N}\psi_2\right)^2} \right]$$

$$Q_{1,2}(\tau) = \frac{1}{2}\left[e^{-\gamma_{1,2}^2\left(\tau - \frac{\pi}{N}\psi_{1,2}\right)^2} + e^{-\gamma_{1,2}^2\left(\tau + \frac{\pi}{N}\psi_{1,2}\right)^2} \right]$$

$$Q_{1,2}^{\star}(\tau) = \frac{1}{2}\left[e^{-\gamma_{1,3}^2\left(\tau - \frac{\pi}{N}\psi_{1,3}\right)^2} + e^{-\gamma_{1,3}^2\left(\tau + \frac{\pi}{N}\psi_{1,3}\right)^2} \right] \tag{8}$$

The constants γ's control the rates of decay while ψ's represent the time shifts. The Fourier transforms of the Q's are then given by

$$\hat{Q}_1(\omega) = \frac{1}{2\gamma_1\sqrt{\pi}}\, e^{-\left(\frac{\omega}{2\gamma_1}\right)^2}$$

$$\hat{Q}_2(\omega) = \frac{1}{2\gamma_2\sqrt{\pi}}\, e^{-\left(\frac{\omega}{2\gamma_2}\right)^2}$$

$$\hat{Q}_{1,1}(\omega) = \hat{Q}_1(\omega) \cos\left(\frac{\omega\pi}{N}\psi_1\right)$$

$$\hat{Q}_{2,2}(\omega) = \hat{Q}_2(\omega) \cos\left(\frac{\omega\pi}{N}\psi_2\right)$$

$$\hat{Q}_{1,2}(\omega) = \frac{1}{2\gamma_{1,2}\sqrt{\pi}}\, e^{-\left(\frac{\omega}{2\gamma_{1,2}}\right)^2} \cos\left(\frac{\omega\pi}{N}\psi_{1,2}\right) \tag{9}$$

$$\hat{Q}_{1,2}^*(\omega) = \frac{1}{2\gamma_{1,3}\sqrt{\pi}} e^{-\left(\frac{\omega}{2\gamma_{1,3}}\right)^2} \cos\left(\frac{\omega\pi}{N}\psi_{1,3}\right)$$

In accordance with our assumption of axisymmetry, we set $\phi_1 = 0°$, and chose the fixed point to be at $\theta_1 = 90°$. The computation of $R_{1,2}(\tau)$ in the meridian plane with $\phi_2 = 0°$ and in the azimuthal plane with $\theta_2 = 90°$ are shown in figures 2 and 3. The number of sources chosen in each ring is 16. The location of the rings are at $\ell_1 = 2D$ and $\ell_2 = 5D$, D is the diameter of the ideal jet taken $= 0.0625$ m corresponding to the diameter of the experimental jet. In addition, the spreading angle connecting the two rings of radius $a_1 = .846D$ and $a_2 = 1.36D$ was chosen to be $10°$ corresponding to a jet spreading half angle.

The broadband cross correlation function (fig. 2) shows the decay and the shift of the peak correlation away from $\tau = 0$ with the increase in separation angle from θ_2 from $\theta_1 = 90°$. The same is observed in the experimental data (ref. 2). The azimuthal broadband cross correlation function, figure 3, shows two results at $\phi_2 = 180°$ corresponding to two different decay rates. One is for a slow decay rate; the sources are compact as is shown by the fact that the cross correlation peak at zero time delay. This is also true for $\phi_2 < 180°$. The second result is for fast decay rates; the peak cross correlation occurs at a time delay different from zero, indicating that the sources are not compact with respect to the acoustic wavelength. In this example, the noncompactness contribution became noticeable only at large separation angle as the cross correlation

approaches 180° separation in a broadband sense. Also, in the experimental results[1] the peak correlation occurs at $\tau \neq 0$ at large separation angle $\phi_2 - \phi_1$ showing the noncompactness of the sources. The fact that the broadband cross correlation is even in τ indicates that statistically the sources are symmetrically placed with respect to the axis of the jet.

The phase of the far-field pressure in the meridian plane is shown in figure 4. Results are plotted in terms of the frequency ω for θ_2 ranging from 80° to 0°. Note that the phase goes to zero with the frequency for all angular separations. This proves that the sources are monopoles, since no net cancellation occurs at any one angle more than at any other as ω goes to zero. Also, note that the initial phase slopes are constant at low ω but varying at higher ω. This is an indication that at lower frequency the radiating field pattern is nearly uniform, while at higher frequencies it is not because the sources are noncompact. From this figure, however, one cannot deduce a priori that the sources are noncompact beyond a certain range of frequencies, without first establishing the phase due to geometrical effects. This problem will be discussed further as part of the inverse problem in section B. In addition, the pattern of the phase variation with ω and θ resembles the measured phase (ref. 2), but with one important difference; namely, that in the experiment the phase for θ_2 less than 50° is nonzero as the frequency approaches zero. This is evidence that the sources in the experimental jet are not monopole. This point also will develop further when comparison is made between the phase of monopoles and quadrupoles in section A-2.

---

[1] Results not yet published show that by filtering out the lower frequency on the original broadband spectra, the peak correlations shift nearly symetrically away from $\tau = 0$.

2. <u>Rings with quadrupoles</u>.- The far-field quadrupole of the pressure P in terms of the far-field angle θ and ϕ and distance r are obtained as linear combinations of the following

$$\frac{d^2}{dx^2} P \sim \left[-\frac{\rho}{c_o^3 r} \frac{d^3 q}{dt^3} \left(t - \frac{\vec{r}}{c_o} \right) \right] \cos^2 \theta$$

$$\frac{d^2}{dxdy} P \sim \left[\right] \cos \theta \sin \theta \cos \phi$$

$$\frac{d^2}{dy^2} P \sim \left[\right] \sin^2 \theta \cos^2 \phi$$

$$\frac{d^2}{dxdz} P \sim \left[\right] \sin \theta \cos \theta \sin \phi$$

$$\frac{d^2}{dydz} P \sim \left[\right] \sin^2 \theta \cos \phi \sin \phi$$

$$\frac{d^2}{dz^2} P \sim \left[\right] \sin^2 \theta \cos^2 \phi \tag{10}$$

where $x = r \cos \theta$; $y = r \sin \theta \sin \phi$; $z = r \sin \theta \sin \phi$

The total contribution of a quadrupole becomes:

$$-\frac{\rho}{c_o^3 r} \frac{d^3 q}{dt^3} \left(t - \frac{\vec{r}}{c_o} \right) \left[a_{11} \cos^2 \theta + a_{12} \cos \theta \sin \theta \cos \phi + a_{22} \sin^2 \theta \cos^2 \phi \right.$$

$$\left. + a_{13} \cos \theta \sin \theta \sin \phi + a_{23} \sin^2 \theta \cos \phi \sin \phi + a_{33} \sin^2 \theta \sin^2 \phi \right]$$

$$= - \frac{\rho}{c_o^3 r} \frac{d^3 q}{dt^3} \left(t - \frac{\vec{r}}{c_o} \right) F(\theta, \phi) \tag{11}$$

We will assume that the coefficients a_{11}, a_{12}, ... a_{33} are independent of t for all quadrupoles on the rings.

We make use of the following relationship:

$$\rho^2 < \left[\frac{d^3 q}{dt^3} (t) \right]_{ij} \left[\frac{d^3 q}{dt^3} \right]_{2j} (t + \tau) > = - \frac{d^6}{d\tau^6} Q(\tau) \tag{12}$$

The coefficient a_1 . . . . a_{33} in $F(\theta, \phi)$ will be adjusted to match with experimental results. The general form of the quadrupole correlation function, equivalent to equation 5, for the monopole becomes:

$$\frac{r^2}{\rho^2} < P_1(t) P_2(\ldots) > = - \frac{r^2}{\rho^2} \left[\frac{d^6}{d\tau^6} R_{1,2}(\tau) \right] \cdot F(\theta_1, \phi_1) F(\theta_2, \phi_2) \tag{13}$$

where $R_{12}(\tau)$ is defined in equation 5.

Computation from the quadrupole model of the phase α and $|\hat{R}_{1,2}(\omega)|/R_{1,1}(\omega)$ using the same meridian plane of the previous model is shown in figures 5 and 6. The phase of the quadrupole differs from that of the monopole by 180° for $\theta_2 < 45°$ as the frequency ω goes to zero. Therefore, the type of singularities radiating sound in the far-field are distinguishable by the behavior of α as ω tends to zero. At higher frequencies one cannot, in general, recognize the type of singularities because of their mutual interaction.

The coherence function for the quadrupole model is shown in figure 6 for four different frequencies. It is clear that at lower frequencies the pattern of the quadrupoles is similar to the measurements made for an axysymmetric jet in reference 3. Indeed the phase together with the coherence function shows what types of quadrupole (namely the coefficients a_{11} . . . . a_{33}) dominate. As the frequency increases the coherence function decays due to randomness.

The data shown in the figure have been obtained when all the correlations function Q_1, Q_2 . . . . Q_{12}, Q_{12}^* are even in τ. It is known, however, that at least in the plane of the jet along the direction of flow the source cross correlation function Q_{12}, Q_{12}^* are not even because of convection effects. This additional effect will not be discussed at this time. The present paper attempts to interpret the results in this simplest form, that is, to study the phase variation due to geometrical effects and compactness for different types of singularities.

In order to study further the relationship between the quadrupole model and the measurements, comparison is also made of the azimuthal cross power spectral density. Only the real part is used since in the model the imaginary part is very small at relatively lower frequencies. The calculated real part of the cross spectral density taken at $\theta_1 = \theta_2 = 90°$, and $\phi_1 = 0°$ is shown in figure 7. The behavior is consistent with the measurements, indicating the quadrupole model may be satisfactorily used to model the singularities in a jet.

B. The Inverse Radiation Problem

A question naturally arises regarding the possibility of using acoustic radiation data to infer the characteristics of the source distribution. Although the difficulty in dealing with this, and other types of inverse problems in physical sciences, lies in the fact that they are in general ill-posed, there may conceivably be some way to utilize the singularity model developed together with the measured radiation field to study the inverse relationship.

Since there are many parameters in the model solution, we examine the solution in the meridian plane, that is $\phi_1 = \phi_2 = 0°$ and $\theta_1 = 90°$. Equation 7 reduces to:

$$
\begin{aligned}
\hat{R}_{1,2}(\omega) = e^{-ik_0\ell_1\cos\theta_2} \Bigg[&\hat{Q}_1(\omega) \sum_{j=1}^{N} e^{-i\cos\phi_j(A_1 + B_1)} \\
&+ \hat{Q}_1(\omega) \sum_{j=1}^{N} \left\{ e^{-i(A_1\cos\phi_j - B_1\cos\phi_{j+1})} \right. \\
&\left. \qquad\qquad + e^{-i(A_1\cos\phi_j - B_1\cos\phi_{j-1})} \right\} \\
&+ \hat{Q}_{1,2}(-\omega) \sum_{j=1}^{N} e^{-i\cos\phi_j(A_2 - B_1)} \\
&+ \hat{Q}^{\star}_{1,2}(-\omega) \sum_{j=1}^{N} \left\{ e^{-i(A_2\cos\phi_{j+1} - B_1\cos\phi_j)} \right. \\
&\left. \qquad\qquad + e^{i(A_2\cos\phi_{j-1} - B_1\cos\phi_j)} \right\} \Bigg]
\end{aligned}
$$

$$+ e^{-ik_o \ell_2 \cos \theta_2} \left[\hat{Q}_2(\omega) \sum_{j=1}^{N} e^{-i \cos \phi_j (A_2 - B_2)} \right.$$

$$+ \hat{Q}_{2,2}(\omega) \sum_{j=1}^{N} \left\{ e^{-i(A_2 \cos \phi_j - B_2 \cos \phi_{j+1})} \right.$$

$$\left. + e^{-i(A_2 \cos \phi_j - B_2 \cos \phi_{j-1})} \right\}$$

$$+ \hat{Q}_{1,2}(\omega) \sum_{j=1}^{N} e^{-i \cos \phi_j (A_1 - B_2)}$$

$$+ \hat{Q}_{1,2}^{*}(\omega) \sum_{j=1}^{N} \left\{ e^{-i(A_1 \cos \phi_j - B_2 \cos \phi_{j-1})} \right.$$

$$\left. \left. + e^{-i(A_1 \cos \phi_j - B_2 \cos \phi_{j-1})} \right\} \right] \quad (14)$$

where

$$k_o = \frac{\omega}{c_o}, \quad A_i = -a_i k_o, \quad B_i = -a_i k_o \sin \theta_2; \quad i = 1,2$$

The second step consists of trying to simplify the above equation by observing the behavior in three domains: i) $k_o a_i \ll 1$, ii) $k_o a_1 \sim 1$, and iii) $k_o a_i \gg 1$

1. <u>Geometrical center of the singularity $k_o a_i \ll 1$.</u> At large wavelength in the limit as $\omega \to 0$, A_i, B_i both are $\ll 1$, the first sum in equation 14 reduces to

$$e^{-ik_o \ell_1 \cos \theta_2} \hat{Q}_1(\omega) \left\{ N + i(A_1 - B_1) \sum_{j=1}^{N} \cos \phi_j \div 0\left[(k_o a_i)^2\right] \right\}$$

$$= e^{-ik_o \ell_1 \cos \theta_2} \hat{Q}_1(\omega) \left\{ N + 0(k_o a_i)^2 \right\}$$

because $\sum_{j=1}^{N} \cos \phi_j = 0$

Using a similar approach for the remaining sums in equation 14 and omitting terms of $0\left((k_o a_i)^2\right)$ we have

$$\hat{R}_{1,2}(\omega) = N\left(\hat{q}_1(\omega) e^{-ik_o \ell_1 \cos \theta_2} + \hat{q}_2(\omega) e^{-ik_o \ell_2 \cos \theta_2} \right) \tag{15}$$

where

$$\hat{q}_1(\omega) = \hat{Q}_1(\omega) + 2\hat{Q}_{1,1}(\omega) + \hat{Q}_{1,2}(-\omega) + 2\hat{Q}_{1,2}^{\star}(-\omega)$$

$$\hat{q}_2(\omega) = \hat{Q}_2(\omega) + 2\hat{Q}_{2,2}(\omega) + \hat{Q}_{1,2}(\omega) + 2\hat{Q}_{1,2}^{\star}(\omega) \tag{16}$$

If we also assume $k_o \ell_j \ll 1$ and neglect the second order term we have

$$\frac{r^2}{\rho^2} \hat{R}_{1,2}(\omega) \sim N\left[\hat{q}_1(\omega)(1 - ik_o \ell_1 \cos \theta_2) + \hat{q}_2(\omega)(1 - ik_o \ell_2 \cos \theta_2) \right]$$

$$\sim N\left[\hat{q}_1(\omega) + \hat{q}_2(\omega) \right] e^{-ik_o \cos \theta_2 \Lambda}$$

$$= \frac{r^2}{\rho^2} |\hat{R}_{1,2}(\omega)| e^{i\alpha_1 \omega} \tag{17}$$

where

$$\Lambda = \frac{\ell_1 \hat{q}_1(\omega) + \ell_2 \hat{q}_2(\omega)}{\hat{q}_1(\omega) + q_2(\omega)}, \quad \alpha_1 = \frac{1}{c_o} \cos \theta_2 \Lambda, \quad |\hat{R}_{1,2}(\omega)| = N\left[\hat{q}_1(\omega) + \hat{q}_2(\omega)\right]$$

The far-field phase α_1 is independent of ω corresponding to the geometrical center of the source (or center of mass). It is the phase due to the geometrical position between sources and far-field measurements. When $\Lambda = 0$, α_1 is zero.

The magnitude $|\hat{R}_{1,2}(\omega)|$ as well as Λ are available from measurements. The behavior of Λ is shown in the sketch. The minimum value corresponds to the fixed microphone located at θ_1, the center of the sources.
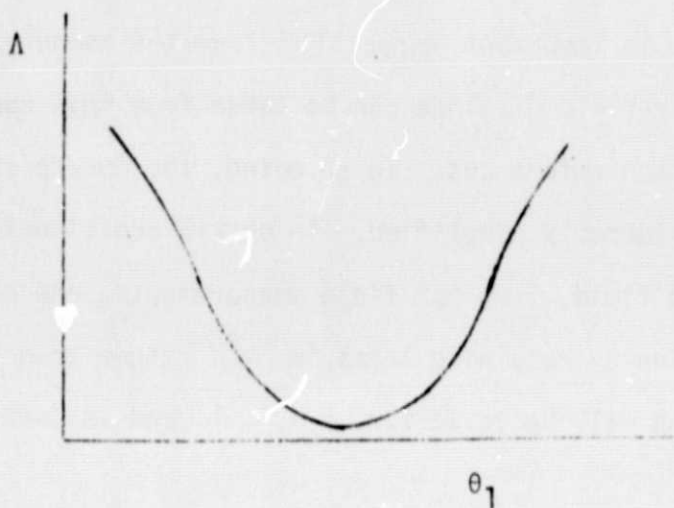
Sketch - Behavior of the geometrical center for fixed far-field angle differences.

In fact, the results show that one can eliminate the phase resulting from the geometry of the orientations. A numerical example is shown in figure 8 where the phases due to monopoles are evaluated with respect to the geometrical center. When the phases are evaluated differently, for example, with respect to a fixed point in the plane of the jet ($\theta_1 = 90°$ shown in fig. 4), the results are radically different than that of figure 8. From the geometrical center the phase at low frequency is zero as predicted by equation 17. The remaining phases as the frequency increases are due to noncompactness of the source, i.e., ring separation, ring diameter, and due to the spacing between sources on the ring.

Equation 17 describes the geometrical center only and cannot provide additional information than what has already been discussed unless $\hat{q}_1(\omega) = \hat{q}_2(\omega)$; in general, however, this is not the case. The geometrical-center result per se is important, especially from the measurement point of view, because the far-field distance can be taken from this center rather than using other center references. In so doing, the interpretation of the results will be considerably simplified. To obtain additional information regarding the source field, from far-field measurements, one can expand the exponentially function by retaining terms in ω^2 rather than in ω only. Such an approximation will be valid for $k_o a_i - 1$ and is carried out in the next subsection.

2. <u>Ring location for $k_o a_i \sim 1$</u>.- Let us expand equation 14 in ω and retain terms of order ω^2 or $k_o^2 a_i^2$. The first term in equation 14 contains $\hat{q}_1(\omega)$, can be written

$$\hat{Q}_1(\omega) \sum_{j=1}^{N} \left\{ 1 - \frac{1}{2} \cos \phi_j \left[A_1(\omega) - A_2(\omega) \right]^2 \right\}$$

$$= \hat{Q}_1(\omega)N - \Omega_1 k_o^2$$

where

$$\Omega_1 = \frac{\hat{Q}_1(\omega)Na_1^2}{4} (1 - \sin \theta_2)^2$$

since $\displaystyle\sum_{j=1}^{N} \cos^2 \phi_j = \frac{1}{2} \sum_{j=1}^{N} (1 + \cos^2 \phi_j) = \frac{N}{2}$

Following the same procedure for the additional seven terms in equation 14, one obtains the following equations for the cross spectral density:

$$\frac{r^2}{\rho^2} \hat{R}_{1,2}(\omega) \sim \hat{q}_1(\omega)e^{-ik_o \ell_1 \cos \theta_2 - \Omega^{(1)}k_o^2}$$

$$+ \hat{q}_2(\omega)e^{-ik_o \ell_2 \cos \theta_2 - \Omega^{(2)}k_o^2} \tag{18}$$

where

$$\Omega^{(1)} = \Omega_1(\omega) + 2\Omega_{1,1}(\omega) + \Omega_{1,2}(-\omega) + 2\Omega_{1,2}^*(-\omega)$$

$$\Omega^{(2)} = \Omega_2(\omega) + 2\Omega_{2,2}(\omega) + \Omega_{1,2}(\omega) + 2\Omega_{1,2}^*(\omega)$$

$$\Omega_{1,1}(\omega) = \frac{\hat{Q}_{1,1}(\omega)Na_1^2}{4} (1 + \sin^2 \theta_2 - 2 \cos \Delta \sin \theta_2)$$

$$\Omega_{1,2}(-\omega) = \frac{\hat{Q}_{1,2}(-\omega)N}{4} (a_2 - a_1 \sin \theta_2)^2$$

$$\Omega_{1,2}^{\star}(-\omega) = \frac{\hat{Q}_{1,2}^{\star}(-\omega)N}{4}\left(a_2^2 + a_1^2 \sin^2 \theta_2 - 2 \cos \Delta\, a_1 a_2 \sin \theta_2\right)$$

$$\Omega_2(\omega) = \frac{\hat{Q}_2(\omega)Na_2^2}{4}\left(1 - \sin \theta_2\right)^2$$

$$\Omega_{2,2}(\omega) = \frac{\hat{Q}_{2,2}(\omega)a_2^2 N}{4}\left(1 + \sin^2 \theta_2\right)^2$$

$$\Omega_{1,2}^{\star}(\omega) = \frac{\hat{Q}_{1,2}^{\star}(\omega)N}{4}\left(a_1^2 + a_2^2 \sin^2 \theta_2 - 2 \cos \Delta\, a_1 a_2 \sin \theta_2\right)$$

and

$$\Omega_{1,2}(\omega) = \frac{\hat{Q}_{1,2}(\omega)N}{4}\left(a_2 - a_1 \sin \theta_2\right)^2$$

Equation 18 can be written as

$$\frac{r^2}{\rho^2}\hat{R}_{1,2}(\omega) = e^{-ik_0\ell_1 \cos \theta_2}\left[\hat{R}_1^{(0)}(\omega) - \frac{1}{4}(k_0 a_1)^2 \hat{R}_1^{(2)}(\omega)\right]$$

$$+ e^{-ik_0\ell_2 \cos \theta_2}\left[\hat{R}_2^{(0)}(\omega) - \frac{1}{4}(k_0 a_2)^2 \hat{R}_2^{(2)}(\omega)\right] \tag{19}$$

where

$$\hat{R}_1^{(0)}(\omega) = \hat{q}_1(\omega); \quad R_2^{(0)}(\omega) = \hat{q}_2(\omega)$$

$$\hat{R}_1^{(2)}(\omega) = \left[\hat{Q}_1(\omega) + 2\hat{Q}_{1,1}(\omega)\right](1 - \sin \theta_2)^2$$

$$+ \left[\hat{Q}_{1,1}(\omega) + \frac{a_2}{a_1}\hat{Q}_{1,2}^{\star}(\omega)\right]4\left(1 - \cos \frac{2\pi}{N}\sin \theta_2\right)$$

$$+ \left[\hat{Q}_{1,2}(-\omega) + 2\hat{Q}^*_{1,2}(-\omega) \right] \left(\frac{a_2}{a_1} - \sin \theta_2 \right)^2$$

$$\hat{R}^{(2)}_2(\omega) = \left[\hat{Q}_2(\omega) + 2\hat{Q}_{2,2}(\omega) \right] (1 - \sin \theta_2)^2$$

$$+ \left[\hat{Q}_{2,2}(\omega) + \frac{a_1}{a_2} \hat{Q}^*_{1,2}(\omega) \right] 4 \left(1 - \cos \frac{2\pi}{N} \right) \sin \theta_2$$

$$+ \left[\hat{Q}_{1,2}(\omega) + 2\hat{Q}_{1,2}(\omega) \right] \left(\frac{a_1}{a_2} - \sin \theta_2 \right)^2$$

Comparisons have been made between the approximation (eq. 19) and the exact solution (eq. 7) at $\theta_1 = 90°$ and $\theta_2 = 30°$ for both phase and absolute value of R. The comparison is shown in table 1 for $N = 16$. The phase up to $\omega = 50,000$ rad/sec varies within 2°; it starts oscillating beyond $\omega = 20,000$. The magnitude $|\hat{R}_{1,2}(\omega)|$ varies about 42 percent at $\omega = 50,000$, corresponding to $a_1 k_o$ of 3.0, while at $\omega = 30,000$ the error in magnitude is only 5 percent corresponding to $a_1 k_o$ of 1.82. Therefore, the approximate solution is useful up to about $ka_1 \sim 2$.

Equation 19 thus contains information not only on the separation distance of the two rings $(\ell_2 - \ell_1)$ but also on the radius of the rings a_1 and a_2. This equation permits the determination of the distance between rings in terms of the compactness behavior of the phase. Since the distance between $(\ell_2 - \ell_1)$ is usually larger than either the radius a_1 or a_2, the first case of non-compactness as the frequency increases occurs at $k_o(\ell_2 - \ell_1) \cos \theta_2 = \pi$, when $\lambda/2 = \ell_2 - \ell_1$; since $k_o = 2\pi/\lambda$. Equation 19 can be written as

ω	$\alpha°$, Exact	$\alpha°$, Approximation	$|\hat{R}_{1,2}(\omega)|$ Exact	$|\hat{R}_{1,2}(\omega)|$ Approximation	$a_1 k_o$	$a_2 k_o$	$(\ell_2-\ell_1)k_o$
1,000	12.94	12.94	21,993	21,993	.06	.097	3.6
3,000	39.11	39.11	80,706	80,705	.18	.29	1.0
5,000	65,60	65.60	89,513	89,507	.30	.48	1.79
7,000	90.90	90.89	116,300	116,280	.43	.68	2.51
10,000	125.20	125.15	123,622	123,519	.6	.97	3.6
15,000	137.084	136.56	48,901	49,353	.913	1.5	5.38
20,000	123.47	124.37	63,450	63,695	1.2	1.9	7.18
30,000	207.42	206.83	14,248	13,584	1.82	2.91	10.0
40,000	284.56	286.52	488	441	2.4	3.9	14.36
50,000	367.49	367.89	5	3.5	3.0	4.8	17.9

Table 1.- Comparison between exact solution and approximation in the limit of $k_o a_1 \leq 1$, at $\theta_1 = 90°$, $\theta_2 = 30°$.

$$\frac{r^2}{\rho^2} \hat{R}_{1,2}(\omega) = \hat{R}_1(\omega)e^{-ik_o\ell_1 \cos\theta_2} + \hat{R}_2(\omega)e^{-ik_o\ell_2 \cos\theta_2}$$

$$= e^{-ik_o\ell_1 \cos\theta_2}\left[\hat{R}_1(\omega) + \hat{R}_2(\omega)e^{-k_o(\ell_2 - \ell_1) \cos\theta_2}\right]$$

$$= e^{-ik_o\ell_1 \cos\theta_2}\left[\hat{R}_1(\omega) - \hat{R}_2(\omega)\right]$$

$$= e^{-i\left(\frac{\ell_1}{\ell_2 - \ell_1}\right)\pi}\left[\hat{R}_1(\omega) - R_2(\omega)\right]$$

$$= A(\omega)e^{-i\left(\frac{\ell_1}{\ell_2 - \ell_1}\right)\pi - i\beta(\omega)} \qquad -\pi < \theta_2 \leq \pi \qquad (20)$$

where

$$\hat{R}_1(\omega) = R_1^{(0)} - \frac{1}{4}\left[k_o\hat{q}_1(\omega)\right]^2 R_1^{(2)}(\omega)$$

$$\hat{R}_2(\omega) = R_2^{(0)} - \frac{1}{4}\left[k_o q_2(\omega)\right]^2 \hat{R}_2^{(2)}(\omega)$$

and

$$\hat{R}_1(\omega) - \hat{R}_2(\omega) = A(\omega)e^{i\beta(\omega)}$$

The phase β is not equal to zero when Q_{12} and Q_{12}^* are not even function of τ. This is a consequence of the non-zero convection velocity of the flow.

For real $\hat{R}_1(\omega)$ and $\hat{R}_2(\omega)$

$$\beta = \begin{cases} 0 & \hat{R}_1(\omega) > R_2(\omega) \\ \pi & R_1(\omega) < R_2(\omega) \end{cases} \qquad (21)$$

The phase of the cross spectral density α is

$$\alpha = \left(\frac{\ell_1}{\ell_2 - \ell_1}\right) \pi + \beta$$

It now becomes

$$\alpha = \left(\frac{\ell_1}{\ell_2 - \ell_1}\right) \pi \qquad \hat{R}_1(\omega) > \hat{R}_2(\omega)$$

α is undefined when $\hat{R}_1(\omega) = \hat{R}_2(\omega)$

$$\alpha = \pi + \left(\frac{\ell_1}{\ell_2 - \ell_1}\right) \pi \qquad \hat{R}_1(\omega) < \hat{R}_2(\omega)$$

Computational results of the phase α in terms of $k_0(\ell_2 - \ell_1) \cos \theta_2$, are shown in figure 9 by equation 14. The phase at all angles θ_2 intercept at $k_0(\ell_2 - \ell_1) \cos \theta_2 = \pi$ with $\alpha = \left(\frac{\ell_1}{\ell_2 - \ell_1}\right) \pi$ since $R_1(\omega) > R_2(\omega)$. This result thus provides additional information toward unraveling the details of the source distribution from far-field measurements.

3. <u>Ring radius $k_0 a_i > 1$</u>.- In order to simplify the higher frequency, expression for large $k_0 a_1$ we use the following approximation for large N

$$\sum_{j=1}^{N} e^{-ik_0 a_i \cos \phi_j} \sim \frac{1}{\Delta} \int_{-\pi}^{\pi} e^{-ik_0 a_i \cos \phi} d\phi$$

$$= \frac{N}{\pi} \int_{0}^{\pi} e^{-k_0 a_i \cos \phi} d\phi = N J_0(k_0 a_i)$$

Since we have $N = 16$ or larger, one can employ this approximation and equation 14 reduces to

$$\hat{R}_{1,2}(\omega) = Ne^{-ik_o\ell_1\cos\theta_2}\left\{\left[\hat{Q}_1(\omega) + 2\hat{Q}_{1,1}(\omega)\cos(B_1\Delta)\right]J_o(A_1 - B_1)\right.$$

$$\left. + \left[\hat{Q}_{1,2}(-\omega) + 2\hat{Q}^*_{1,2}(-\omega)\cos(A_2\Delta)\right]J_o(A_2 - B_1)\right\}$$

$$+ Ne^{ik_o\ell_2\cos\theta_2}\left\{\left[\hat{Q}_2(\omega) + 2\hat{Q}_2(\omega)\cos(B_2\Delta)\right]J_o(A_2 - B_2)\right.$$

$$\left. + \left[\hat{Q}_{12}(\omega) + 2\hat{Q}^*_{12}(\omega)\cos(B_2\Delta)\right]J_o(A_1 - B_2)\right\} \quad (22)$$

When $k_o a_1 \sim 1$ the power series expansion for J_o can be used to recover the results of the previous subsection.

For high frequencies, i.e., $k_o a_i \gg 1$, we note from physical reasoning that

$$\ell_2 - \ell_1 \gg a_i$$

$\hat{R}_{1,2}(\omega)$ reduces to

$$\hat{R}_{1,2}(\omega) \sim Ne^{-ik_o\ell_1\cos\theta_2}\left[\hat{Q}_1(\omega) + 2\hat{Q}_1(\omega)\cos(B_1\Delta)\right]J_o(A_1 - B_1)$$

$$+ Ne^{-ik_o\ell_2\cos\theta_2}\left[\hat{Q}_2(\omega) + 2\hat{Q}_{2,2}(\omega)\cos(B_1\Delta)\right]J_o(A_2 - B_2)$$

Since the acoustic energy of high frequency decays with distance downstream
from the jet exit,

$$\hat{Q}_1(\omega) \gg \hat{Q}_2(\omega) > Q_{2,2}(\omega)$$

Therefore we have

$$\hat{R}_{1,2}(\omega) \sim Ne^{-ik_o \ell_1 \cos \theta_2} \left[\hat{Q}_1(\omega) + 2\hat{Q}_{1,1}(\omega)\cos(B_1\Delta)\right] J_o(A_1 - B_1) \tag{23}$$

The magnitude of the cross spectral density function vanishes when

$$A_1 - B_1 = k_o a_1(1 - \sin \theta_2) = \nu_m$$

where ν_m is the m-th root of $J_o(z)$

A plot of the normalized absolute value $|\hat{R}_{1,2}(\omega)|/\hat{R}_{1,1}(\omega)|$ is shown in
figure 10. Note that the first two zeros occur at $k_o a_1 = 2.4$ and 5.52 when
the magnitude of the far-field pressure reaches a minimum. At lower value of
$k_o a_1$ the undulation of the coherence function is due to cancellation
resulting from the matching of the acoustic wavelength with distance between
rings. This effect occurs at $k_o a \leq 1$, a problem discussed previously.

In order to confirm this cancellation effect the numerical results have
been compared with results based on the first four zeros of the Bessel function
of order zero, as obtained from tables. The results of this comparison is
presented in table 2.

$k_o a_1$ from table	$k_o a_1$ computed	ω rad/sec
2.405	2.403	38,300
5.520	5.520	87,977
8.654	8.653	137,900
11.792	11.790	187.900

Table 2.- Comparison of $k_o a_1$ calculated from zeros of the Bessel function $J_o(k_o a) = 0$ with results computed from the monopole model.

The agreement is excellent, indicating that the coherence function or the absolute value can be utilized in obtaining information on the source radius. The radius of the second ring a_2 is generally not directly available from the absolute value of the far-field pressure, but to improve the signal one can search for it in the plot of the coherence.

There are also other ways to determine the radius a_2. One is by assuming a spreading angle between the two rings based on physical reasoning. Thus, from the far-field correlation the location and the diameters of the rings, as well as the type and compactness of the sources, can be extracted. The results are given in table 3. In order to better assess the validity of the approximate solution, additional comparisons of phase and magnitude values were made for a large range of ω.

CONCLUSION

This paper contains the solution of a direct and an inverse problem on the radiation of sound from randomly fluctuating sources on two rings. This work concentrated on obtaining the properties of the signals originating

ω rad/sec	α exact	α approx.	$\lvert R_{12}(\omega) \rvert$ exact	$\lvert R_{12}(\omega) \rvert$ approx.
50,000	-116.017	-115.989	3.9003	4.0821
60,000	- 30.875	- 30.875	2.6190	2.6448
70,000	54.004	54.004	3.8417	3.8017
80,000	138.863	138.863	1.12398	1.0762
90,000	43.721	43.721	5.6892	6.6684
100,000	128.579	128.579	2.0669	2.1127
110,000	-146.563	-146.563	6.9836	7.0143
120,000	- 61.705	- 61.705	5.3225	5.2844
130,000	23.153	23.153	8.2173	7.9814
140,000	- 71.990	- 71.990	2.2542	2.5394
150,000	12.868	12.868	4.2972	4.3947
160,000	97.726	97.727	7.6057	7.7301
170,000	-177.416	-177.416	2.9407	3.0221

Table 3.- Comparison between exact and approximate solution: $k_o a_1 > 1$, at $\phi_2 = 0°$, N = 16.

from a random medium with known statistical properties. From the inverse radiation approach which utilizes the memory of the received signals associated with the distortion, several questions regarding physical interpretation of the signals in relationship to its origin have been clarified. In particular, the interpretation of data related to phase and coherence functions permits the establishing of: (1) the center of mass of the singularities, (2) the geometrical shape and size, and (3) the ability to distinguish one type of singularity from another and from it determine the basic directivity of the different components. In addition, from the signals one can (4) deduce the distribution of the singularities either when compact or noncompact with respect to the acoustic wavelength.

The location of the center of mass is an important factor to establish in an experiment, otherwise error can easily result, inadvertently, especially at those frequencies in which the far-field distance becomes geometrically limited.

The results presented are mainly related to the meridian plane. Additional information comes from the simultaneous observations of both azimuthal and meridian planes with $Q_{1,2}(\tau)$ taken as an odd function of the time delay τ. This information together with the partial recovery of the functions Q's will not be discussed at this time.

REFERENCES

1. Ribner, H. S.: Two Point Correlations of Jet Noise. J. Sound and Vibration, vol. 56, no. 1, 1978, pp. 1-19. NASA TN D-8330, 1976.

2. Maestrello, L.: Two Point Correlations of Sound Pressure in the Far-Field of a Jet: Experimental. NASA TM X-72835, 1976.

3. Maestrello, L.: Statistical Properties of the Sound and Source Fields of an Axisymmetric Jet. AIAA Paper 77-1267, 1977.

4. Maestrello, L.; and Liu, C. H.: Jet Noise Source Distribution for Far-Field Cross Correlation. AIAA, vol. 15, no. 6, 1977.

5. Chow, P. L.; and Maestrello, L.: Stochastic Inverse Problems in the Radiation of Noise. To be published in the SIAM Journal.

6. Fisher, M. J.; Harper-Borne, M.; and Glegg, S. A. L.: Jet Engine Noise Source Location: "The Polar Correlation Technique." J. Sound and Vibration, vol. 51, no. 1, 1977, pp. 23-54.

7. Chu, W. T.; Laufer, J.; and Kao, K.: Noise Source Distribution in Subsonic Jet. International Conference on Noise Control, Washington, DC, October 1972, pp. 472-476.

8. Grosche, F. R.: Distributions of Sound Source Intensities in Subsonic Jet. AGARD Conference, CP-31, 1973.

9. Perulli, M.: Comparaison de Differentes Methodes de Localisation et D'Identification de Sources Sonores de Turboreacteurs. AGARD LPS-80, Aerodynamic Noise, November 1976.

10. Michalke, A.: On the Effect of Spatial Source Coherence on the Radiation of Jet Noise. J. of Sound and Vibration, vol. 55, no. 3, 1977, pp. 377-394.

11. Hadamark, J.: Lectures on Cauchy's Problems in Linear Partial Differential Equations, Dover, New York, 1952.

12. Ribner, H. S.: Aerodynamic Noise from Fluid Dilatation. University of Toronto, UTIAS Report 86, 1962.

13. Ffowcs Williams, J. E.: The Noise from Turbulent Convection at High Speed. Philosophical Transactions of the Royal Society, London A255, 1963, pp. 469-503.
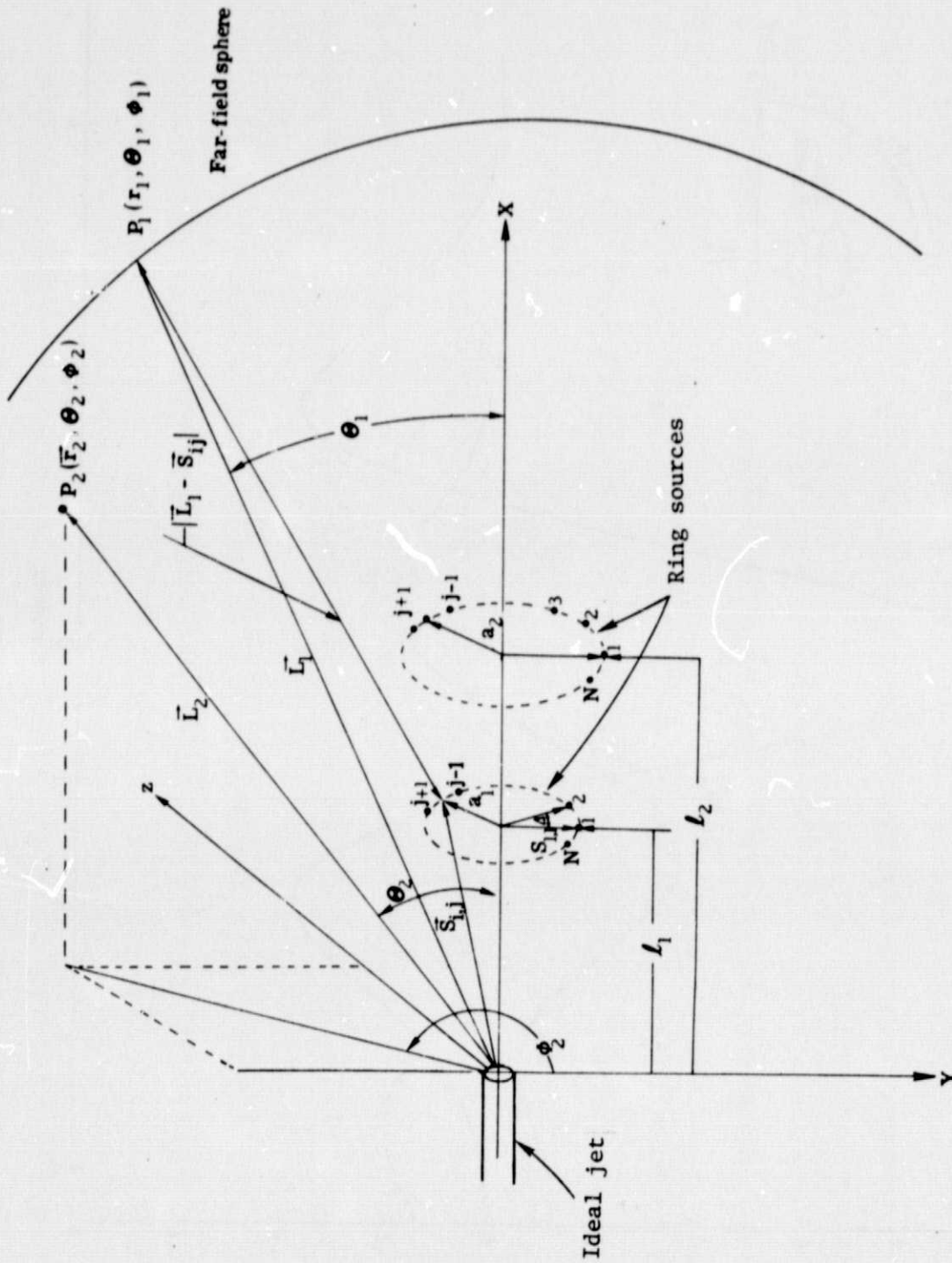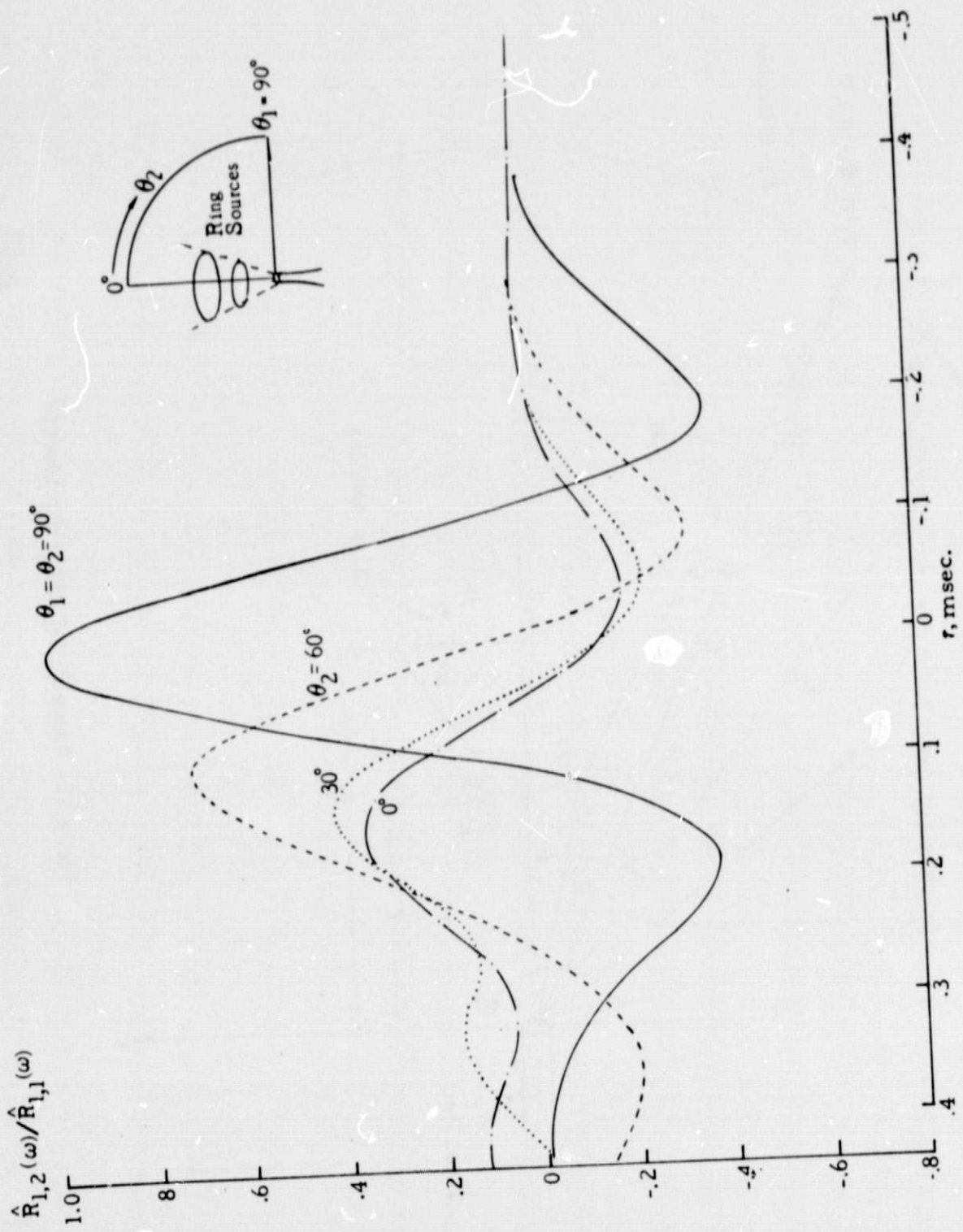
Figure 1.- Geometry of the ring sources.

Figure 2.- Broadband correlation for monopole in the meridian plane.
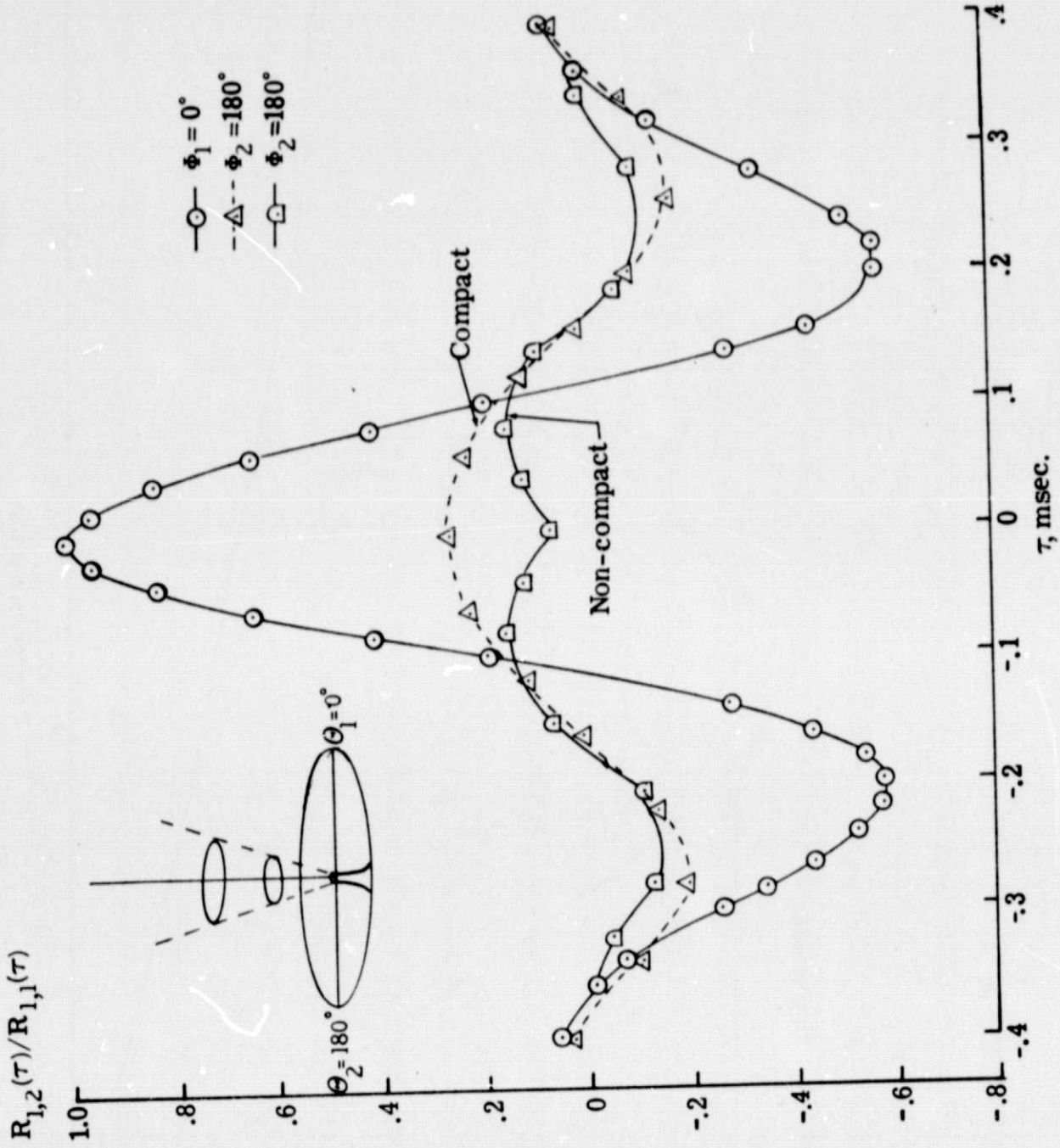
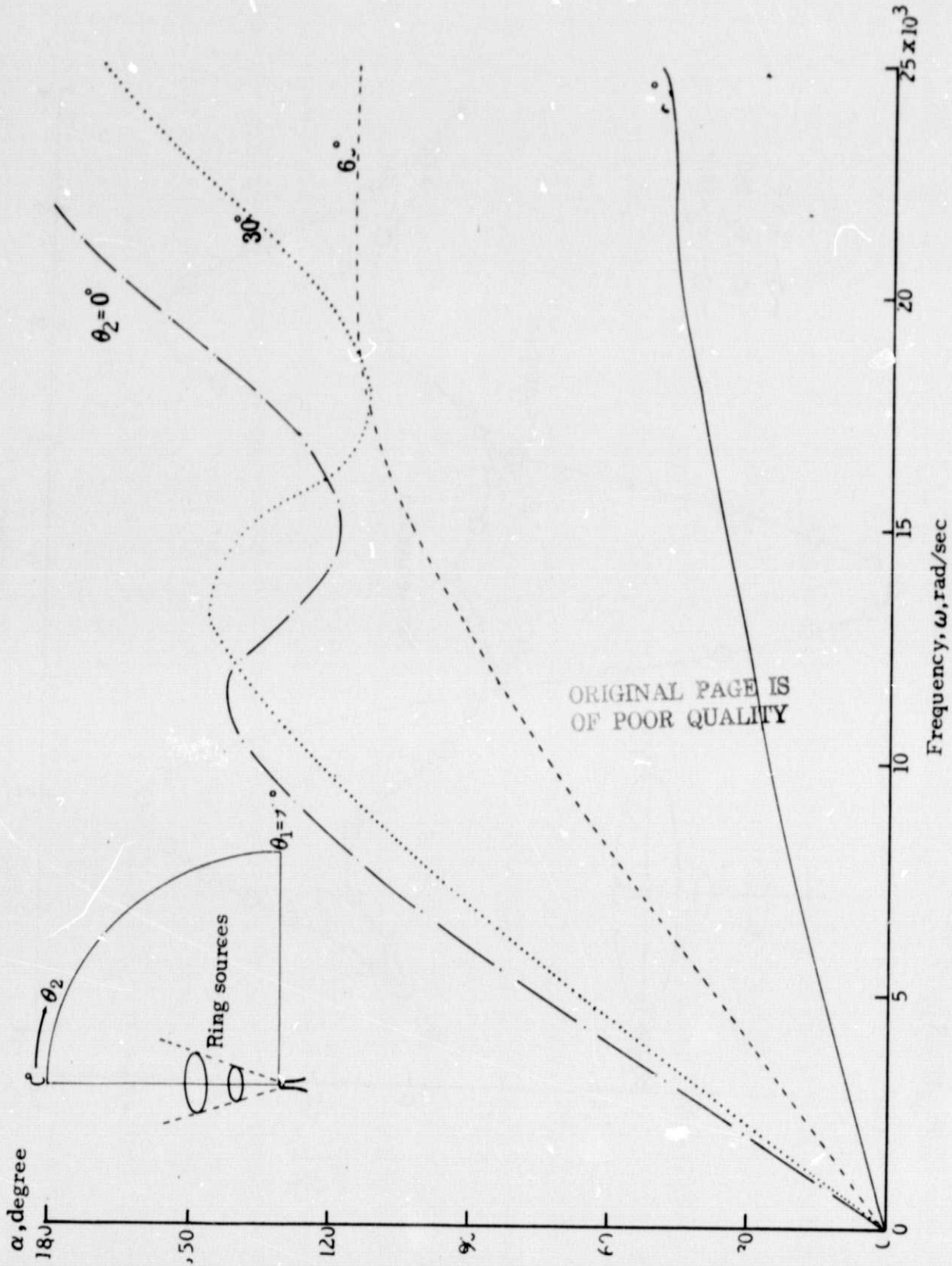Figure 3.- Broadband cross correlation for monopole in the azimuthal plane.

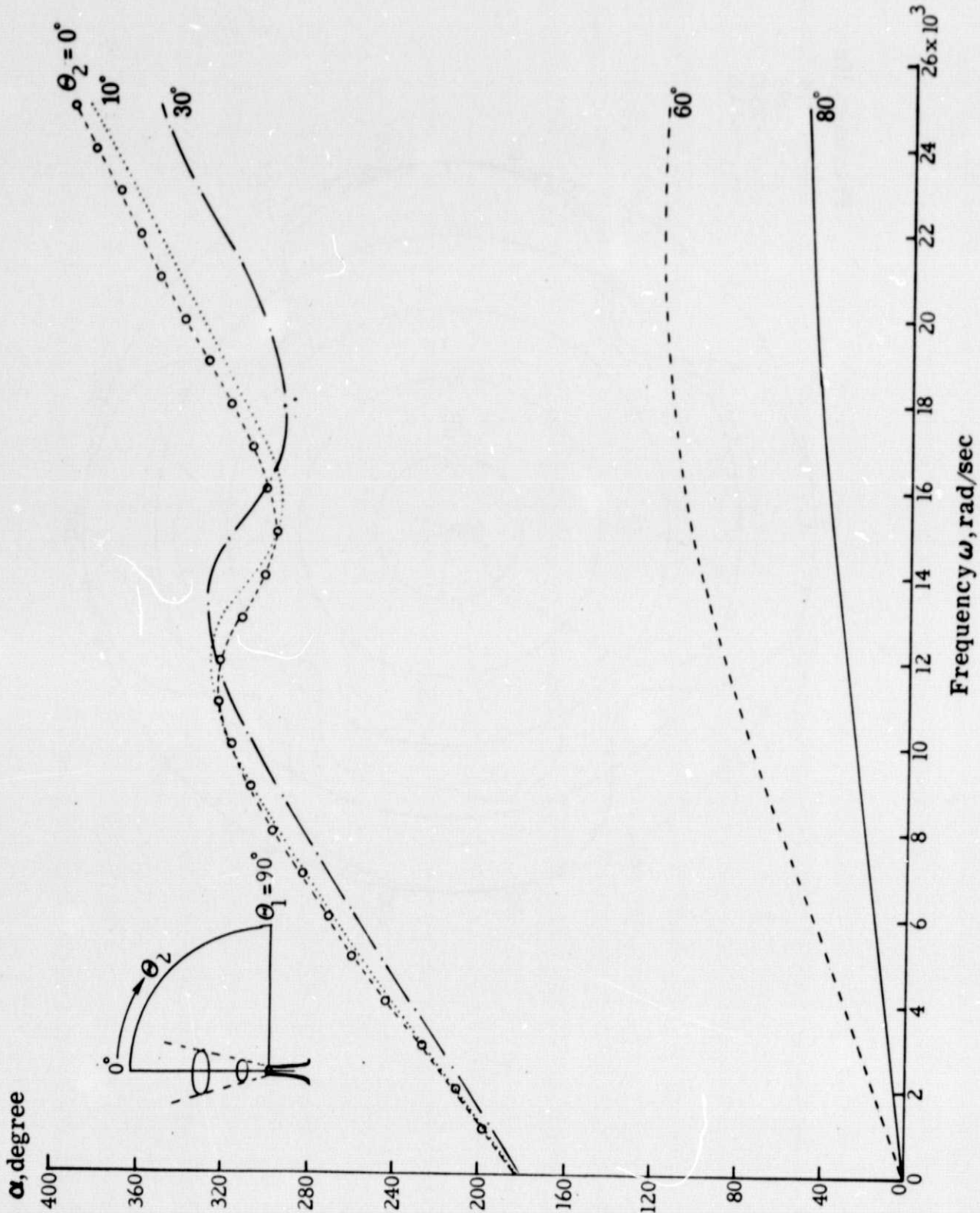Figure 4.- Far-field phase for monopole in the meridian plane.

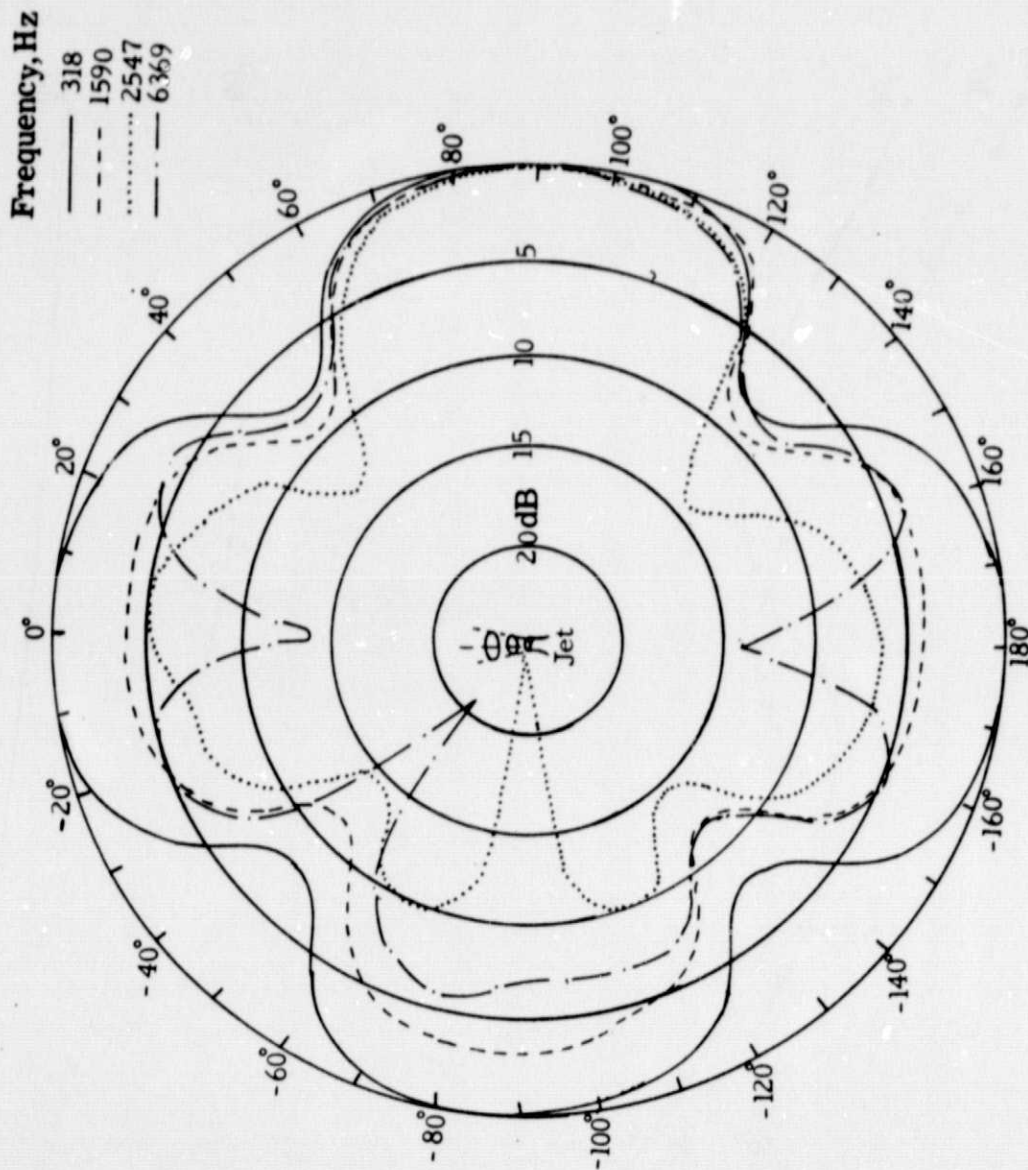Figure 5.- Far-field phase for quadrupole in the meridian plane.

Figure 6.- Coherence function for quadrupole in the meridian plane $|\hat{R}_{1,2}(\omega)|/P_1(\omega)P_2(\omega)$.
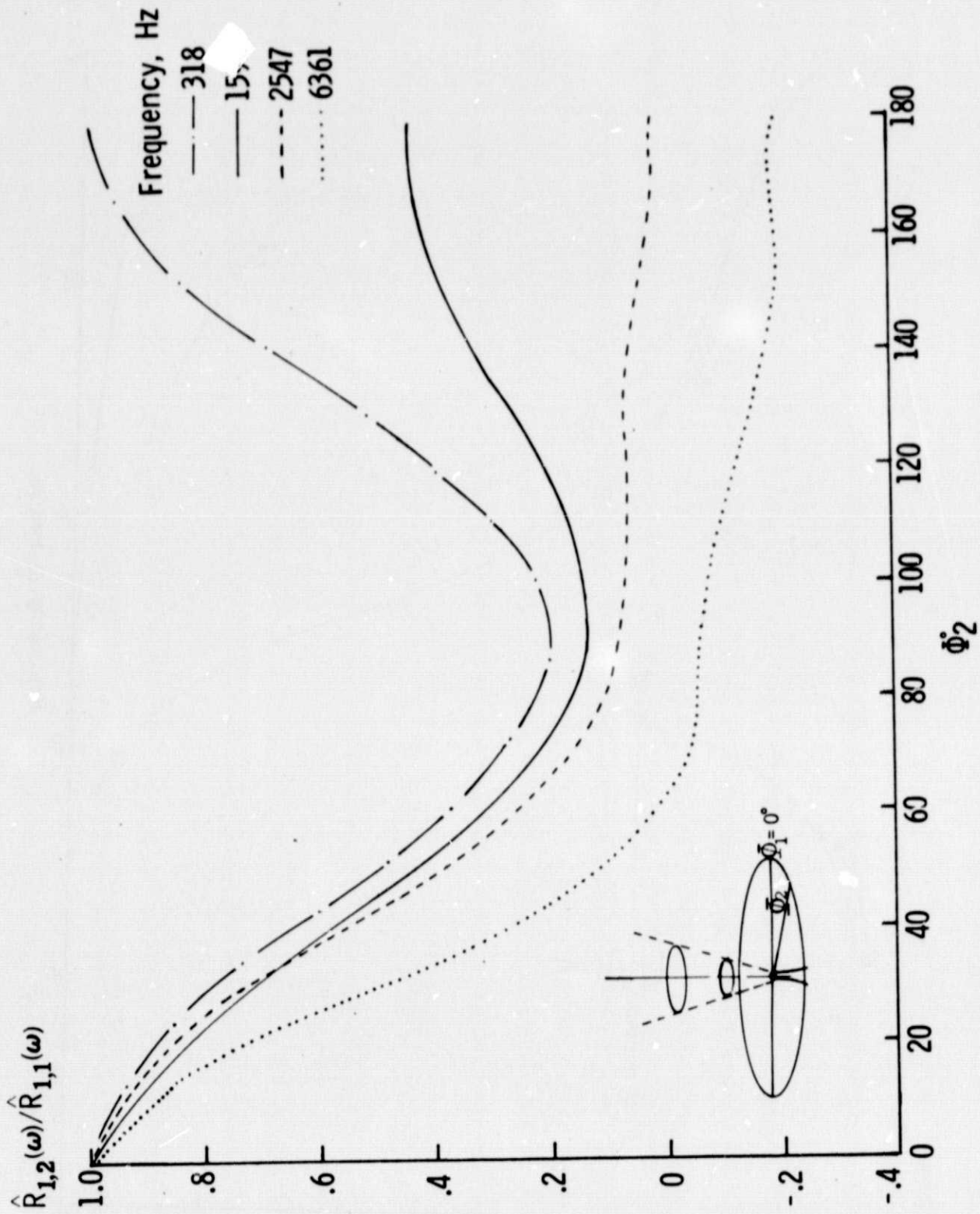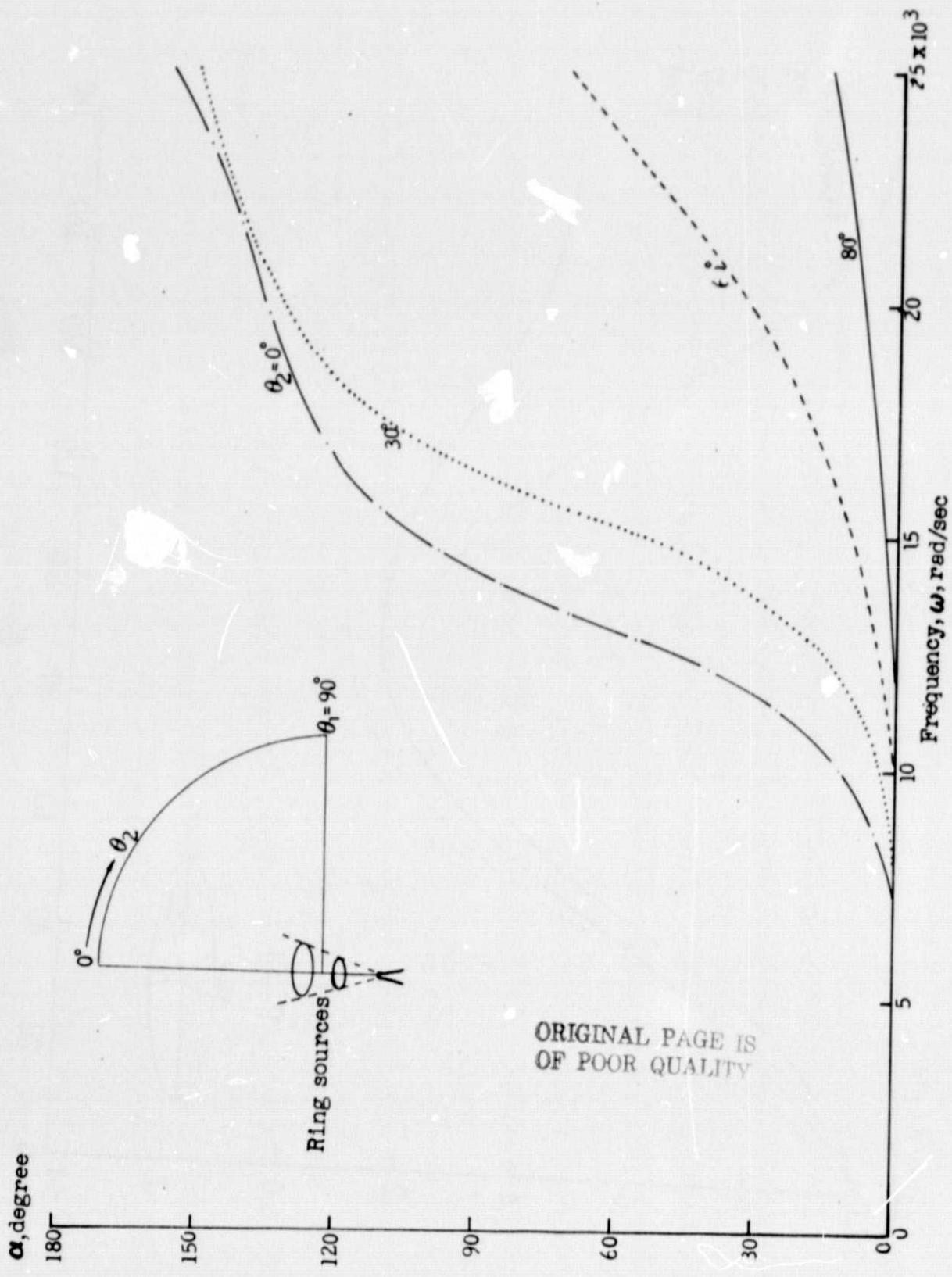
Figure 7.- Real part of the cross spectral density in the azimuthal plane.

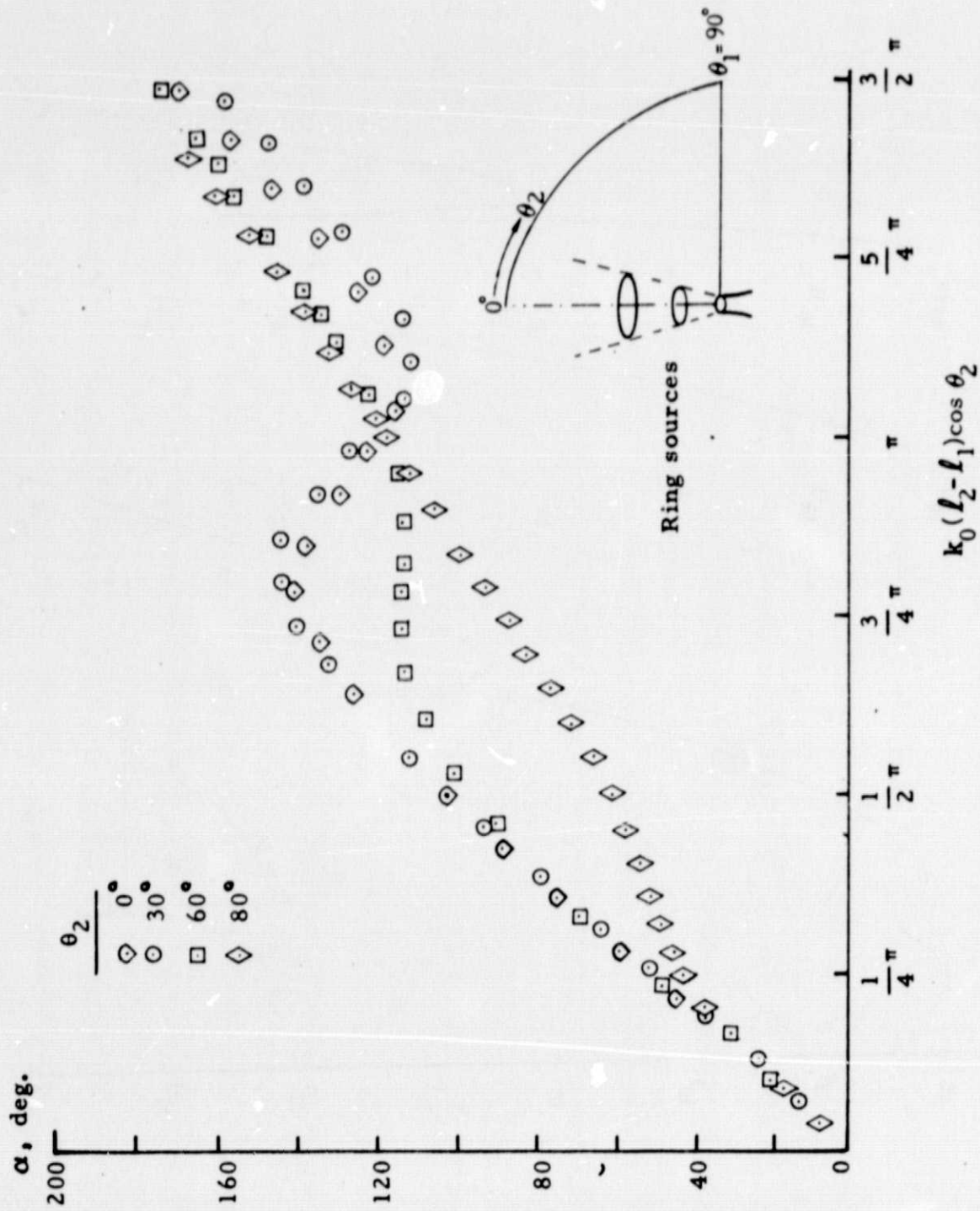Figure 3.- Far-field phase for monopole about the center of mass in the meridian plane.

Figure 9. – Far-field phase for monopole with specified rings separation in the meridian plane.
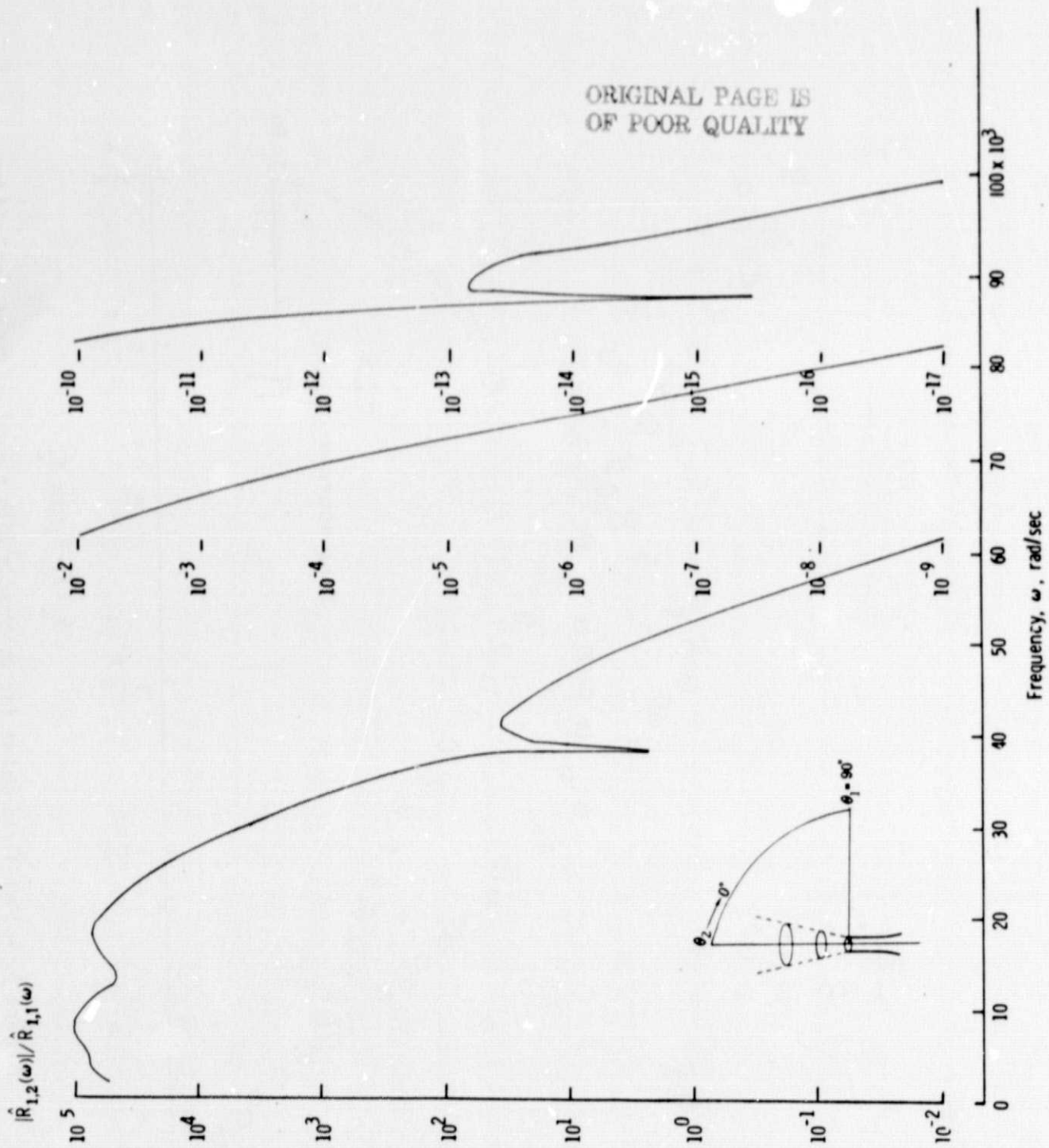
Figure 10.- Magnitude of the far-field pressure for monopole $\theta_1 = 0°$, $\theta_2 = 90°$

1. Report No. NASA TM-73959	2. Government Accession No.	3. Recipient's Catalog No.
4. Title and Subtitle A Ring-Source Model for Jet Noise		5. Report Date April 1978
		6. Performing Organization Code
7. Author(s) Lucio Maestrello		8. Performing Organization Report No.
		10. Work Unit No.
9. Performing Organization Name and Address NASA Langley Research Center Hampton, VA 23665		11. Contract or Grant No.
		13. Type of Report and Period Covered Technical Memorandum
12. Sponsoring Agency Name and Address National Aeronautics and Space Administration Washington, DC 20546		14. Sponsoring Agency Code

15. Supplementary Notes

Presented at the 95th Meeting of the Acoustical Society of America, Providence Rhode Island, May 14-19. 1978

16. Abstract

A model consisting of two ring sources has been developed to study the direct radiation of jet noise in terms of correlation, coherence, and phase and also to aid in solving the inverse radiation problem of determining the noise source in terms of far-field measurements. The rings consist of discrete sources which are either monopoles or quadrupoles with Gaussian profiles. Only adjacent sources, both within the rings and between rings, are correlated. Results show that from the far-field information one can determine when the sources are compact or noncompact with respect to the acoustic wavelength and distinguish between the types of sources. In addition, from the inverse radiation approach, one can recover the center of mass, the location and separation distance of the ring, and the diameters.

17. Key Words (Suggested by Author(s)) Jet Noise Direct Radiation Inverse Radiation	18. Distribution Statement Unclassified - Unlimited Subject Category 71
19. Security Classif. (of this report) Unclassified	20. Security Classif. (of this page) Unclassified	21. No. of Pages 40	22. Price* $4.50